1   **Title: IL15/IL15Rα complex induces an anti-tumor immune response following radiation**

2   **therapy only in the absence of Tregs and fails to induce expansion of progenitor TCF1+**

3   **CD8 T cells**

4

5   **Authors:** Miles Piper*, Jacob Gadwa*, Chloe Hodgson*, Michael Knitz, Elliott Yee, Yuwen Zhu,

6   Keira Y. Larson, Christian Klein, Maria Amann, Anthony Saviola, Sana D Karam

7

8   **Keywords**: Immunotherapy; radiation; pancreatic cancer; cytokines; IL15; cytotoxic T

9   lymphocytes; NK cells; Tregs

10

11   **Declarations of Interest**

14

15   **Abstract**

16   Background: This work seeks to understand whether IL15-incorporating treatments improve

17   response to radiotherapy and uncover mechanistic rationale for overcoming resistance to IL15

18   agonism using novel therapeutic combinations.

19   Experimental Design: Orthotopic tumor models of PDAC were used to determine response to

20   treatment. IL15-/- and Rag1-/- mouse models were employed to determine dependence on IL15

21   and CTLs, respectively. Flow cytometry was used to assess immune cell frequency and

22   activation state. Phospho-proteomic analyses were used to characterize intracellular signaling

23   pathways.

24   Results: We show that the combination of radiation therapy (RT) and an IL15/IL15Ra fusion

25   complex (denoted IL15c) fails to confer anti-tumor efficacy; however, a CD8-driven anti-tumor

26 immune response is elicited with the concurrent administration of an aCD25 Treg-depleting

27 antibody. Using IL15-/- and Rag1-/- mice, we demonstrate that response to RT + IL15c + aCD25

28 is dependent on both IL15 and CTLs. Furthermore, despite an equivalent survival benefit

29 following treatment with RT + IL15c + aCD25 and combination RT + PD1-IL2v, a novel

30 immunocytokine with PD-1 and IL2Rβγ binding domains, CTL immunophenotyping and

31 phospho-proteomic analysis of intracellular metabolites showed significant upregulation of

32 activation and functionality in CD8 T cells treated with RT + PD1-IL2v. Finally, we show the

33 immunostimulatory response to RT + PD1-IL2v is significantly diminished with a concurrent lack

34 of TCF+ CD8 T cell generation in the absence of functional IL15 signaling.

35 Conclusions: Our results are illustrative of a mechanism wherein unimpeded effector T cell

36 activation through IL2Rβ signaling and Treg inhibition are necessary in mediating an anti-tumor

37 immune response.

38

39 **Introduction**

40   Despite treatment advances in surgery, chemotherapy, and radiation therapy (RT),

41 pancreatic adenocarcinoma (PDAC) remains a devastating disease with a stagnant 5-year

42 overall survival rate of 12%S. With few available treatment options, RT has been pursued as an

43 adjuvant and neoadjuvant therapeutic in locally advanced and metastatic PDAC[1]. However, the

44 widespread use of RT remains controversial, with radiation-induced fibrosis suggested as a

45 possible correlate of worsened survival outcomes in some cases[2,3]. Further complicating

46 treatment, many studies in the field of radiobiology have shown high dose RT delivered in large

47 fractions increases the infiltration and activation of immunosuppressive regulatory T cells

48 (Tregs) in locally advanced PDAC tumors[4], and simultaneously fails to induce infiltration of CD8

49 T cells and natural killer (NK cells) critical for an anti-tumor immune response[4,5], highlighting the

50 narrow therapeutic utility for RT in the treatment of PDAC in current practice.

51   Despite these potential negative sequelae and the overall lack of immune infiltration

52   following RT alone, studies have shown RT can enhance the effect of immunostimulatory

53   treatments through the disruption of tumor vasculature and the release of proinflammatory

54   cytokines and chemokines[6], making it an attractive combinatorial option for immunomodulatory

55   regimens. Moreover, recent studies have shown that the potential benefits of including RT in

56   immunotherapeutic treatments extend beyond tumor lymphocyte infiltration. In our previous

57   work, we demonstrated a synergistic effect of combination RT with the novel immunocytokine

58   PD1-IL2v, which delivers variant interleukin-2 (IL-2) to PD1-expressing T cells while also

59   inhibiting PD-1 signaling[7]. We established that the novel combination of RT + PD1-IL2v

60   treatment not only increases cytotoxic T lymphocyte (CTL) frequency and polyfunctionality in

61   both the tumor and draining lymph nodes, but also improves systemic immune surveillance and

62   increases overall survival in orthotopic murine models of PDAC[7]. The RT + PD1-IL2v

63   combination also resulted in the generation of a tumor-specific memory response that remained

64   durable upon tumor rechallenge[7], thus advocating for a role for RT in mediating a robust anti-

65   tumor immune response when rational combinations are pursued.

66   Sharing many binding and signaling properties with PD1-IL2v, another emerging

67   cytokine in the field of cancer immunobiology that has garnered much attention due to its ability

68   to induce CD8 T cell memory and NK cell development and cytotoxicity is interleukin 15 (IL-15)[8].

69   Like PD1-IL2v and other IL2R-modulating agents, IL15 is a member of the common gamma

70   chain family of cytokines and therefore has a strong impact on CTL functionality[8]. IL15 receptor

71   signaling is unique in that it requires binding of IL15 to IL-15Rα on innate immune cells followed

72   by subsequent cross-presentation of the IL15/ IL-15Rα complex to IL-2Rβγ on target cells[9],

73   allowing for tight regulation of endogenous IL15-mediated activation. To combat this signaling

74   peculiarity, recombinant IL-15 complexed with IL-15Ra ex vivo is currently being explored as a

75   therapeutic option due to its longer half-life, more profound expansion of CD8 T cells and NK

76   cells, and overall reduction in tumor burden[10]. In this work, we evaluated the use of the IL-15/IL-

77   15Ra complex (denoted IL-15c) in combination with RT while simultaneously managing RT-

78   mediated Treg expansion using an aCD25 depletion antibody as a treatment strategy in PDAC

79   tumors.

80

81   **Results**

82   **Combination RT + IL15c is inefficacious; the addition of aCD25 to the RT + IL15c regimen**

83   **prolongs overall survival and enhances CTL activation**

84   To begin our analysis, we first sought to understand the translational potential of IL15

85   agonist therapies by interrogating RNA sequencing data from a previously published dataset of

86   SBRT-treated PDAC patient tumor samples (GEO: GSE225767)[7]. We found that responders to

87   SBRT alone exhibited elevated intratumoral levels of IL-15 transcripts prior to treatment (**Fig**

88   **S1A**) and IL15 was among the most frequently appearing genes in the significantly upregulated

89   pathways in responders relative to non-responders, appearing in 5 out of 10 pathways (**Fig**

90   **S1B**).

91   Next, given the dependency of IL-15 signaling on the trans-presentation of IL-15Rα by

92   innate cells to IL-2Rβγ on target cells (**Fig 1A**), we assessed the efficacy of our IL15 complex

93   (see Methods) using an *in vitro* cytotoxicity assay (**Fig 1B**). We found that NKs stimulated with

94   IL15c induced significantly more cancer cell death over control and that IL15c was more or

95   equally effective in inducing cancer cell death compared to either IL2 or standard IL15 (**Fig 1C**).

96   To characterize the effect of IL15c agonism *in vivo*, we next utilized Kras-driven orthotopic tumor

97   PDAC models and treated tumor-bearing mice with RT and/or combination IL15c (**Fig 1D**).

98   Given the central role of Tregs in mediating disease recurrence, particularly in the context of

99   RT[5], a treatment arm including a Treg-depleting aCD25 antibody was also included (**Fig 1D**).

100 We found that neither RT + IL15c nor RT + aCD25 improved overall survival compared to RT

101 alone (**Fig 1E**). However, the addition of aCD25 to RT + IL15c treatment did result in a

102 significantly increased overall survival compared to RT (HR=3.8; p value=0.0017) and

103   combination RT + IL15c (HR=4.9; p-value=0.0001), suggesting combination RT and IL15

104   agonism may have a clinical utility but only in the context of a Treg-deficient system (**Fig 1E**).

105   As metastatic disease burden is highly prevalent in pancreatic cancer patients with over

106   50% of patients presenting with metastatic disease to the liver at the time of diagnosis[11,12], we

107   next explored the efficacy of the RT + IL15c + aCD25 regimen in a hemi-spleen metastatic

108   model of PDAC using Kras-driven murine cell line[13] (**Fig S1C**). As before, we observed a lack of

109   response following RT + IL15c treatment relative to RT alone; however, the triple combination of

110   RT + IL15c + aCD25 resulted in reduced metastatic disease burden and prolonged overall

111   survival (HR=2.72; p-value=0.026) (**Fig S1D**).

112   To understand the mechanism of the improved response to combination RT + IL15c +

113   aCD25 treatment, we performed flow cytometry on lymphocytes harvested from the blood and

114   tumor of PDAC tumor-bearing mice. We found that animals treated with a regimen including

115   IL15c had a significant expansion of circulating NK cells compared to control (**Fig 1F**), and NK

116   cells treated with IL15c had significantly increased expression of IFNγ, DNAM-1, and GnzmB

117   (**Fig 1G**). We also found that mice treated with RT + IL15c + aCD25 had significantly increased

118   frequency of circulating CD8 T cells (**Fig 1H**), as well as increased CD44+ and

119   IFNγ+/GnzmB+/TNFa+ polyfunctional CD8 T cells (**Fig 1I**). Importantly, mice treated with triple

120   RT + IL15c + aCD25, the group with the best response rate (**Fig 1E**), had the lowest levels of

121   intratumoral Tregs (**Fig 1J**), highlighting the importance of Treg depletion in mediating response

122   to treatment.

123

124   **Response to RT + IL15c + aCD25 is dependent on CTLs and functional IL15 signaling**

125   As sustaining the memory CD8 T cell population is a well-described defining feature of

126   IL15 signaling[14], we sought to determine whether the observed survival benefit following RT +

127   IL15c + aCD25 triple combination treatment is dependent on the maintenance of the CD8

128   population. Utilizing the Rag1-/- mouse model lacking functional T and B cells (**Fig 2A**), we

129   found that orthotopic tumor-bearing Rag1-/- mice treated with triple combination RT + IL15c +

130   aCD25 had a median survival of 19.5 days as compared to 32 days in wildtype C57/BL6 mice

131   treated with RT + IL15c + aCD25 (HR=4.09; p value=0.0001) (**Fig 2B**).

132   We then sought to determine the dependence of the improved response to RT + IL15c +

133   aCD25 treatment on IL15 signaling specifically. To do this, we utilized a globally deficient IL15

134   (IL15-/-) mouse model[15] (**Fig 2C**). As seen in the wildtype system, RT + IL15c and RT + aCD25

135   resulted in no improvement in overall survival over RT alone. However, supplementation of

136   aCD25 to the RT + IL15c treatment was able to significantly enhance survival benefit in an IL15-

137   deficient system (HR=3.7; p-value=0.0031) (**Fig 2D**). Next, to characterize the circulating

138   cellular populations contributing to the response to RT + IL15c + aCD25 in both WT C57/BL6

139   and IL15-/- mice, we used flow cytometric analysis of circulating immune cells and found a

140   significant reduction in the frequency of NK and CD8 T cells in IL15-/- mice treated with RT

141   compared to WT mice treated with RT (**Fig 2E-F**). However, both NK and CD8 T cell frequency

142   and activation (as evidenced by NKG2D and CD44 expression, respectively) were restored with

143   the addition of aCD25 and IL15c in the WT and IL15-/- mouse models (**Fig 2E-F**). Importantly,

144   this restoration was associated with a concurrent decrease in CD45-/EpCAM+ circulating tumor

145   cell (CTC) frequency, whereas the reduction in CTLs in the IL15-deficient system was

146   associated with a significant increase in CTCs (**Fig 2G**). These data suggest that functional IL15

147   signaling is critical to enhancing CTL maturation and differentiation, reducing disease burden,

148   and improving overall survival in response to RT + IL15c + aCD25 treatment.

149   Finally, to test the direct cytotoxic potential of CTLs following IL15c stimulation, we

150   performed an *in vitro* cytotoxicity assay with NK cells isolated from WT and IL15-/- mice and

151   treated them *in vitro* with IL-15c. We found that although NKs maturing in an IL15-deficient

152   system have a lower baseline level of cytotoxicity, treatment with IL15c was able to significantly

153   improve their cytotoxic potential (**Fig 2H**).

154

RT + PD1-IL2v is superior to RT + IL15c + aCD25 in inducing immune activation, overall survival

The beta subunit of the IL2R receptor has recently garnered substantial interest as a target of selective agonism in anti-tumor immunity[9]. Our group and others have shown that PD1-IL2v, a novel immunocytokine consisting of an aPD-1 blocking antibody conjugated to an IL-2 variant optimized for IL-2Rβγ binding, robustly expands antigen-specific, TCF1+ anti-tumor T cells and leads to a significant survival benefit with RT and aPD-L1 combinations[7,16,17]. Because the IL15 signaling axis also utilizes IL2Rβ[9], we next sought to characterize the differences in response to IL15c and PD1-IL2v treatments. Using an orthotopic model of PDAC (**Fig 3A**), we found that treatment with RT + PD1-IL2v resulted in a superior increase in overall survival relative to RT + IL15c treatment (HR=1.8, p-value=0.078) (**Fig 3B**).

Using multicompartmental flow cytometry, we then aimed to characterize the immune changes in response to each treatment. Through this analysis, we found that when compared to RT and RT + IL15c treatment, circulating CD8 T cells in animals treated with RT + PD1-IL2v more frequently expressed the activation markers CD44 (**Fig 3C**) and IFNγ (**Fig 3D**), and later in the disease course (24 days post-implantation), these animals also had a higher proportion of CD8 T cells expressing CD27 and EOMES (**Fig 3E**). Meanwhile, CD8 T cells in the draining lymph nodes of mice treated with RT + PD1-IL2v had significantly upregulated IFNγ and TNFα expression and an increased frequency in PD1+/TCF1+ stem-like memory CD8 T cells[18] (**Fig 3F**). Within the tumor, RT + PD1-IL2v treated animals showed a profound increase in infiltrating CD8 T cells (**Fig 3G**). Analysis of the activation and functional potential of tumor-infiltrating CD8s showed that those treated with RT + PD1-IL2v had significantly increased GnzmB+ and KLRG1+/CD127+ CD8 T cells, as well as a trend toward increased memory precursor effector CD8 T cells (MPECS)[19] (**Fig 3H**), altogether suggesting that although RT + IL15c + aCD25 treatment increases the frequency of CTLs and depletes the immunoinhibitory Treg population,

180 treatment with RT + PD1-IL2v is far superior in inducing CTL expansion and activation and

181 increasing overall survival.

182

183 RT + PD1-IL2v treatment induces significantly more phosphorylation of activation

184 pathways in CD8 T cells than RT + IL15c + aCD25

185 Given the superior immunostimulatory effect of RT + PD1-IL2v relative to RT + IL15c +

186 aCD25 despite operating on overlapping signaling axes, we hypothesized that while IL-15c and

187 PD1-IL2v both interact with IL-2Rβγ on CD8 T cells, the differences in response to RT + PD1-

188 IL2v and RT + IL15c treatment are due to disparate activation of CD8 T cell signaling cascades.

189 To explore the phenotypic differences in CTLs following IL15c and PD1-IL2v administration, we

190 performed phosphoproteomic analysis (see Methods, **Supp Fig 2A**) on circulating CD8 T cells

191 harvested and isolated from tumor-bearing mice treated with RT, RT + IL15c + aCD25, and RT +

192 PD1-IL2v (**Fig 4A**). We began our analysis with hierarchal and unsupervised clustering of

193 samples from each treatment group which showed unique clustering patterns and distinct

194 differences in phosphosite expression (**Fig 4 B-C**). Volcano plots of differentially expressed

195 phosphosites were then generated and showed CD8 T cells treated with RT + PD1-IL2v had

196 significantly more phosphorylated metabolites relative to control than those treated with RT +

197 IL15c + aCD25, suggesting PD1-IL2v is superior to IL15c in initiating intracellular activation (**Fig

198 4D**).

199 We then shifted our analysis to individual phosphorylated proteins and found significant

200 upregulation of a number of phosphosites in CD8 T cells from tumor-bearing mice treated with

201 RT + PD1-IL2v, most notably those related to T cell signaling and activation pathways (**Figure

202 4E**). For example, we found increased phosphorylation at S42 of Lck, necessary for integrin-

203 mediated signaling in T cells[20], and increased S21 of Fyn, involved in cell migration[20]. Various

204 residues also showed increased phosphorylation in Lat, downstream of Zap70, suggestive of

205 superior TCR signaling (**Fig 4E**). Meanwhile, Ctnnb1 (beta-catenin) showed decreased

206   phosphorylation at S191, which may indicate a polarization toward an effector rather than

207   memory phenotype[21,22]. Phosphorylation was also decreased at the inhibitory residue Y15 of

208   Cdk1, suggesting that T cell expansion may be increased and T cell anergy decreased in CD8 T

209   cells treated with RT + PD1-IL2v[23,24] (**Fig 4E**). Together, these data suggest that the unique

210   stimulatory properties of the PD1-IL2v immunocytokine are highly effective at inducing the

211   intracellular activation of CTLs and highlight the inherent limitations of endogenous signaling

212   molecules as a form of anti-tumor treatment.

213

214   **Response to RT + IL15c treatment is not improved with the addition of immune**

215   **checkpoint blockade**

216   Given the divergent responses to RT + IL15c + aCD25 and RT + PD1-IL2v treatment, we

217   next hypothesized that the inferiority of IL15-incorporating therapies is due to a lack of

218   concurrent immune checkpoint inhibition. To test this claim, we orthotopically implanted

219   pancreatic tumors into wildtype mice and treated them with RT + IL15c and RT + IL15c + aPD1.

220   We then performed flow cytometry on peripheral and intratumoral immune populations and

221   compared those findings to tumor-bearing mice treated with RT + PD1-IL2v (**Fig 5A**). We found

222   RT + PD1-IL2v resulted in a trend toward reduced tumor size at day 23 post-implantation as

223   compared to RT + IL15c + aPD1 (p-value=0.39) (**Fig 5B**).

224   Using flow cytometry to analyze peripheral immune populations, we found that mice

225   treated with RT + PD1-IL2v had a significantly increased frequency of CD8 T cells relative to

226   every other treatment group, including RT + IL15c + aPD1 (**Fig 5C**). Analysis of the activation

227   state of these CTLs showed significantly more expression of IFNg, TNFa, and TCF1 (**Fig 5D**) in

228   mice treated with RT + PD1-IL2v, suggesting enhanced activity and reduced exhaustion of CTLs

229   in these animals. Of note, RT + PD1-IL2v resulted in similar levels of Treg frequency, as defined

230   by CD4+/CD25+ cells, despite a significant increase in pro-inflammatory markers (**Fig S3A**). We

231   also found that although RT + PD1-IL2v did not result in a significant expansion of the NK cell

232 compartment as was observed in the RT + IL15c group (**Fig 5E**), RT + PD1-IL2v did induce

233 significantly more expression of GnzmB, DNAM1, and IFNg in peripheral NK cells as compared

234 to each other treatment arm (**Fig 5F**).

235   When looking at the intratumoral immune infiltrate, we found that the frequency of CD8 T

236 cells was significantly increased in mice treated with RT + PD1-IL2v as compared to RT + IL15c

237 + aPD1, as well as each other treatment group (**Fig S3B**). Moreover, tumor-infiltrating GnzmB+

238 and TNFa+ CD8 T cells were significantly increased and there was a trend toward increased

239 IFNg production in mice treated with RT + PD1-IL2v (**Fig 5G**). Finally, mice treated with RT +

240 PD1-IL2v had a significantly increased intratumoral frequency of PD1+/TCF1+ progenitor

241 exhausted CD8 T cells, a CD8 subpopulation associated with increased stemness and self-

242 renewal[25] (**Fig 5H**). Altogether these findings suggest RT + PD1-IL2v combination treatment

243 confers some functional advantage over RT + IL15c + aPD-1 despite shared PD-1 blockade and

244 IL-2Rβγ signaling receptor agonism.

245

246 **IL15 signaling is necessary for durable response to RT + PD1-IL2v treatment**

247   Because PD1-IL2v induces such a profound and systemic activation of CD8 T cells, one

248 would reason that functional IL15 signaling is necessary to attain a maximal response to RT +

249 PD1-IL2v treatment. As such, we next utilized our IL15-/- to test whether the response to RT +

250 PD1-IL2v is dependent on IL15 signaling (**Fig 6A**). Using this model, we observed a significant

251 reduction in overall survival following RT + PD1-IL2v treatment in IL15-/- mice when compared

252 to their WT C57/BL6 counterparts (HR=4.47; p=0.0005) (**Fig 6B**). The addition of IL15c,

253 however, rescued the effect of RT + PD1-IL2v treatment in the IL15-/- mouse model, as tumor-

254 bearing mice treated with RT + PD1-IL2v + IL15c had a significantly improved survival over mice

255 treated with RT + PD1-IL2v (HR=2.7; p-value=0.402) (**Fig 6C**). This suggests that PD1-IL2v

256 requires an intact IL15 signaling axis to mediate a durable and systemic anti-tumor immune

257 response.

258   To understand the impact of IL15 signaling on the response to RT + PD1-IL2v treatment,

259   we then implanted orthotopic PDAC tumors into IL15-/- and used flow cytometry to characterize

260   circulating immune populations before and after the initiation of RT + PD1-IL2v as compared to

261   RT + IL15c + aCD25 treatment (**Fig 6D**). We found that mice treated with RT + PD1-IL2v RT +

262   IL15c + aCD25 similarly induced expansion of Ki67+ NK cells (**Fig 6E**), decreased levels of

263   CD62L+ and EOMES+ CD8 T cells, and increased levels of EOMES+/CD27+ and EOMES-

264   /Tbet+ CD8 T cells (**Fig 6F**). Interestingly, however, only RT + PD1-IL2v + IL15c resulted in a

265   significant increase in EOMES+/Ki67+ and TCF+ CD8 T cells relative to RT + PD1-ILv treatment

266   (**Fig 6G-H**), suggesting IL15 agonism may provide a unique contribution to the durable

267   response via induction and maintenance of the central memory CD8 T cell population[26,27].

268   Finally, we asked the question of whether RT + PD1-IL2v therapy could be further

269   improved with the addition of concurrent IL15c administration. Although the addition of IL15c to

270   RT + PD1-IL2v combination treatment did not significantly improve median survival over RT +

271   IL15c, RT + PD1-IL2v + IL15c treatment did lead to a complete response in some animals, with

272   2 of 14 mice living past 110 days post-implantation free of tumor burden (**Fig 6I**).

273

Discussion

275   Due to the overlapping intracellular involvement of JAK1, JAK3, and STAT3/5[9], and

276   importantly extracellular involvement of IL2R$\beta\gamma$, many studies have been performed to

277   understand the commonalities between IL2 and IL15 signaling, with results consistently showing

278   that IL2 has a more prominent role in the initiation of an immune response functioning as a T

279   cell growth factor and promoting the maintenance of self-tolerance, whereas IL15 is critical to a

280   longer-lasting high-avidity T cell response involving the induction of CD8 memory T cells[9].

281   These effects would lead one to believe that cytokine-based therapies involving the

282   administration of purified or recombinant IL2 and IL15 would elicit a significant anti-tumor effect.

283   Such treatments, however, have been shown to come with their own set of challenges, including

284   dose-limiting toxicity, off-target effects, and suboptimal efficacy[28]. To address these

285   shortcomings, novel fusion proteins, such as IL15/IL15Ra complexes, have recently been

286   developed and found to have enhanced biological activity, a longer half-life, and improved

287   disease control in preclinical models[10]. In fact, IL15c therapies have shown so much promise

288   that they are now making their way to the clinic, with the IL-15R agonist ALT-803/N-803 in

289   combination with BCG now approved as a treatment modality in muscle-invasive BCG-

290   unresponsive bladder cancer[29], and IL15R agonist in combination with pembrolizumab or

291   standard of care in stage III/IV NSCLC[30]. In this study, we sought to understand 1.) whether

292   these novel approaches involving IL15 agonism can improve the response to RT in preclinical

293   models of PDAC and 2.) whether IL15 agonism is superior to IL2 agonism, and in particular the

294   novel PD1-IL2v immunocytokine[7], in promoting an anti-tumor immune response and improving

295   overall survival.

296   Our data show that unlike the combination of RT and PD1-IL2v, the addition of IL15c to

297   RT is devoid of any additional antitumoral efficacy over RT alone and fails to confer a T effector

298   immune response. Despite significantly enhancing NK and CD8 T cell activation, we show that

299   the lack of effect following RT + IL15c treatment is driven primarily by regulatory T cells as

300   further addition of a Treg-depleting aCD25 antibody to RT + IL15c elicited a significant anti-

301   tumoral response approaching that of RT + PD-IL2v. Moreover, using the Rag1-/- mouse model

302   lacking functional T cells, we show that Treg inhibition is necessary but not sufficient in

303   mediating a systemic immune response to the RT + IL15c + aCD25 treatment regimen and

304   response requires the presence of activated CTLs. Translationally, these findings advocate for

305   the concurrent targeting of Tregs in therapies incorporating IL15 agonism as the beneficial

306   effects of IL15 agonism are significantly impeded by Treg-mediated immunosuppression.

307   Although the topological structures of IL2Rα (CD25) and IL15Rα (CD215) have been

308   shown to be nearly identical[9], the ability of PD1-IL2v to preferentially stimulate IL2Rβγ on CTLs

309   while subverting IL2Rα agonism on Tregs is one possible explanation for its superior efficacy[7].

310 In this work, through mechanistic studies characterizing the differences in response to IL15c

311 and PD1-IL2v, we also identified a key role for CD8 stem cells, without which a durable immune

312 response is not possible and without which the immunocytokine PD1-IL2v cannot generate an

313 anti-tumoral systemic immune response. Interestingly, by utilizing an IL15-/- mouse model, we

314 show that this potent CD8-driven antitumoral immune response is dependent on the presence of

315 IL15 and, without it, no TCF+ CD8 T cells can be generated and all response to RT + PD1-IL2v

316 combination treatment is lost. Moreover, our phospho-proteomics analysis of CD8 T cells

317 derived from RT + PD1-IL2v and RT + IL15c + aCD25 tumor-bearing mice, in concordance with

318 findings by others, show that although the IL2 and IL15 signaling pathways share the IL2Rβγ

319 complex, treatment of T cells with high concentration IL2 and IL15 results in differential

320 intracellular signaling and tnf, Ifng, and Il2ra gene expression[31]. Together, these results identify

321 the generation of CD8 stem cells as a necessary pre-requisite for the generation of effective

322 anti-tumoral immune response and are suggestive of a mechanism wherein unimpeded effector

323 T cell activation following IL2 agonism is necessary in the acute anti-tumor immune response,

324 whereas IL15 signaling plays an important role in the generation of a systemic and durable

325 immunity.

326 Of note, the idea of utilizing a bifunctional signaling molecule to provide IL15-mediated

327 immunostimulation while simultaneously inhibiting immunosuppression does have precedent in

328 the literature. In a recent study by Liu et. al., the group describes the creation and biological

329 activity of a heterodimeric bifunctional fusion molecule composed of soluble TGFβ-R and

330 IL15/IL15Rα domains (HCW9218) as a novel immunotherapeutic agent with both IL15-mediated

331 immunostimulatory and TGFb antagonistic activities[32]. They show that this molecule significantly

332 enhances NK and CD8 T cell activation and infiltration, reduces circulating plasma TGFβ levels,

333 and improves disease control. Meanwhile, Xu et. al. recently generated an IL15-mutein and

334 PD1-specific antibody fusion complex (aPD1-IL15m) and demonstrated that this molecule was

335   more biologically active than either of its components alone. They found that aPD1-IL15m

336   robustly enhances the proliferation, activation, and cytotoxicity of CTILs and improves anti-

337   tumor immunity[33]. The results described in our work would seem to validate these studies while

338   going further to establish a role for radiation in such combinatorial approaches and emphasizing

339   the importance of IL2-mediated generation of TCF1+ CD8 T cells in generating a durable

340   response to treatment.

341   Collectively, our data reinforce the now widely understood differences between IL2 and IL15

342   signaling and highlight the important differences between IL2 and IL15 in mediating the acute

343   and chronic anti-tumor immune response. These results also advocate for the use of RT when

344   used in the appropriate setting and will help guide future clinical trials exploring IL2Rβ-

345   modulating agents in novel combinations.

346

347   **Acknowledgements**

352

353   **Materials and Methods**

354   **Patients and samples**

355   Written consent was obtained for all tumor sample collection. Studies were performed in

356   accordance with U.S. Common Rule and approved by institutional review board. Patient archival

357   tumor samples were identified and obtained from the University of Colorado PSR biorepository

358   and collected per COMIRB13-0315. Samples were selected from all borderline resectable

359   pancreatic cancer patients seen through University of Colorado pancreatic multidisciplinary

360   clinic between 1/2013–12/2018 and were treated with FOLFIRINOX or gemcitabine based

361 neoadjuvant chemotherapy and stereotactic body radiotherapy (SBRT). Following neoadjuvant

362 therapy, all patients received surgery followed by further adjuvant chemotherapy.

Cell lines and reagents

364 PK5L1940 mouse pancreatic adenocarcinoma cell line was kindly provided by Dr. Michael

365 Gough (Providence Cancer Institute, Portland, OR). FC1242 mouse pancreatic adenocarcinoma

366 cell line was kindly provided by Dr. David Tuveson (Cold Spring Harbor Laboratory, Cold Spring

367 Harbor, NY). Cell lines were passaged in RPMI1640 supplemented with 10% FBS every 2–3

368 days at a density of 1:4-1:10. Cells were not allowed to grow beyond passage 30.

Mice

370 Female C57BL6 (6-8 weeks old) and Rag1-/- (B6.129S7-Rag1tm1Mom/J) (6-8 weeks old) were

371 purchased from Jackson Laboratories (Indianapolis, In, USA). IL15-/- mice were kindly provided

372 by Dr. Ross Kedl (University of Colorado, Denver, CO).

373 All mice were cared for in accordance with the ethical guidelines and conditions set and

374 overseen by the University of Colorado, Anschutz Medical Campus Animal Care and Use

375 Committee. Protocols used for animal studies were reviewed and approved by the Institutional

376 Animal Care and Use Committee at the University of Colorado, Anschutz Medical Campus.

377 Experimental unit size was determined using historical results to maximize statistical

378 significance and minimize animal death (n=3-6 per group for flow cytometry studies; n=7-12 for

379 survival studies). Mice were randomized into treatment groups on day 6 post-implantation, prior

380 to the initiation of treatment. All experimental mice were included in survival and

381 immunophenotyping studies.

Local and metastatic pancreatic adenocarcinoma implantations

383 Local orthotopic implantations were conducted by first anesthetizing mice using isoflurane and

384 making a 1 cm incision in the left subcostal region. Mouse pancreata were located, externalized,

385 and injected with 200,000 PK5L1940 or FC1242 KPC cells suspended 1:1 in Matrigel (Corning,

386 Corning, NY). Pancreata were then reintroduced into abdomen and mice peritoneum and skin

387 were closed. Protocol described in further detail[34] . Survival and flow cytometric in vivo studies

388 were conducted and analyzed separately.

389 Metastatic orthotopic implantations were conducted as above with spleen externalization

390 following subcostal incision. Spleens were first ligated with horizon clips and 1 hemispleen was

391 injected with 200,000 FC1242 cells suspended in 50µl 10% RPMI followed by washout injection

392 of 50 µl PBS. Pancreatic vessels were then ligated with horizon clips and hemispleen was

393 excised prior to closure of peritoneum and skin. Metastatic implantation described in further

394 detail[13]. For cancer specific mortality, mice determined to have died from other causes were

395 excluded from the analysis.

396 ***In vivo* drug administration**

397 aCD25 (Roche Pharmaceuticals, 3mg/kg), PD1-IL2v (muPD1-IL2v, Roche Pharmaceuticals,

398 0.5mg/kg)[16], and DP47-IL2v (muDP47-IL-2v) (0.5mg/kg) were administered intraperitoneally

399 once per week beginning one week after tumor implantation. aPD-1 (BioExcell, 10 mg/kg) was

400 administered intraperitoneally twice per week beginning one week after tumor implantation

401 consistent with the previously published protocol[7]. IL15c was generated by mixing recombinant

402 IL-15 with recombinant IL-15Ra at a m/m ratio of 1:10 and incubated for 30 minutes at 37C prior

403 to administration. IL-15c (0.4mg/kg) was administered intraperitoneally twice per week

404 beginning one week after tumor implantation.

405 **Flow cytometry**

406 For flow cytometric analysis of tumor tissue, tumors were digested into single-cell suspension as

407 previously reported[35]. Briefly, tumors were finely cut and incubated in HBSS solution with

408 Collagenase III (Worthington) at 37°C. After incubation, tumors were passed through a 70 µm

409 nylon mesh. The resulting cell suspension was centrifuged and re-suspended in red blood cell

410 (RBC) lysis buffer for 5 minutes. RBC lysis buffer was deactivated, cell suspensions were

411 centrifuged, re-suspended, and counted using an automated cell counter. Tumor-draining

412 inguinal lymph nodes and spleens were processed into single-cell suspensions as above. For

413   flow cytometric analysis, cells were plated in 24-well plates and cultured for 4 hours in the

414   presence of monensin, PMA, and ionomycin to stimulate cytokine production and block Golgi

415   transport. Cells were then blocked with anti-CD16/32 antibody. Where necessary, cells were

416   fixed and permeabilized prior to staining using the FoxP3 Fixation/Permeabilization protocol

417   (eBioscience). Samples were run on the Cytek Aurora Spectral Cytometer at the Barbara Davis

418   Center at the University of Colorado Diabetes Research Center (NIDDK grant #P30-DK116073).

419   Data were analyzed using FlowJo Analysis software. Populations were visualized using

420   FlowSOM within Cytobank software.

421   **Radiotherapy**

422   Image-guided radiotherapy was performed using the X-Rad SmART small animal irradiator

423   (Precision X-Ray, North Bradford CT) at 225kVp, 20mA with 0.3 mm Cu filter. Mice were

424   positioned in the prone orientation and a CT scan was acquired. Radiation was delivered at a

425   dose rate of 5.6Gy/min. A single 8 Gy dose of X-ray radiation was delivered to mouse pancreata

426   using 10mm square beam with field edges at mouse midline and below left ribs. Monte-Carlo

427   simulation was performed using SmART-ATP software (SmART Scientific Solutions, Maastricht,

428   Netherlands) with a CBCT scan of one mouse to determine the appropriate time and current. All

429   mice received identical treatment after repositioning by fluoroscopy. For all in vivo experiments,

430   radiation was given at 7 days post-implantation as previously described[7].

431   **In Vitro Calcein Release Assay**

432   Cytotoxicity assay was performed by pre-staining PK5L1940 pancreatic cancer cell lines using a

433   2mg/ml calcein solution and isolating NK cells according to the manufacturer's protocol. Briefly,

434   cancer cells were incubated in calcein-containing media for 30 minutes at 37C and

435   subsequently plated in a 96-well plate at a 2:1 NK cell to cancer cell ratio. The reaction mixture

436   was then allowed to incubate at 37C for 4 hours. Following the incubation period, supernatant

437   was collected and cancer cell release of calcein was quantified by fluorescence (Ex: 485nm/EM:

438   530 nm) Protocol described in further detail[36].

Phospho-proteomics/phospho-array

Samples were prepared for mass spectrometry using S-Trap^{TM} micro filters (Protifi, Huntington, NY) according to the manufacturer's protocol. Phosphopeptides were enriched using the Fe-NTA Phosphopeptide Enrichment Kit (ThermoFisher Scientific) and subjected to liquid chromatography tandem mass spectrometry using a NanoElute liquid chromatography system coupled with a timsTOF SCP mass spectrometer (Bruker, Germany). Raw spectra were interpreted against the UniProt *Mus musculus* protein sequence database using MSFragger with a false discovery rate of <1.0%. Phosphoproteomics data was analyzed using R as follows. Intensity data collected with phosphosites in rows and samples in columns was filtered to only include rows with phosphorylation events: rows with assigned modifications including a weight change +79.9663 Da. Some data rows included multiple modifications per quantified peptide; these rows were separated vertically so that each row would include intensity of a single peptide phosphorylation event per row. Positions of modifications were shown in original data relative to the start of each peptide sequence identified; these positions were converted to an absolute position relative to the entire peptide sequence of matched protein ID, which allowed for identification with known phosphorylation events documented in the literature. Rows at this point that mapped to the same protein-phosphosite pair were combined by sum, such that each row showed sample intensities for sites of the format *<gene symbol>;<residue><position>;* for phosphorylation events at serine, threonine, or tyrosine residues. Further data shaping as follows: Rows were filtered out if in intensity was constant across the entire row for all samples. Values with expression zero were interpreted as missing not at random, as missing values occurred with lower intensity, suggesting dropouts for lack of detection under a low threshold (see density plot in **Fig S2A**). Rows were then only kept if non-missing intensity was detected in at least 50% of replicates (at least 3 of 5 replicates in a group) within at least one condition (RT, RT + IL15c + aCD25, or RT + PD1-IL2v) using the selectGrps() function with R package PhosR[37,38]. Variance-stabilizing normalization was applied with values returned on the log2

465 scale with R package vsn[39] with functions vsn::vsnMatrix() and vsn::predict() with log2scale =

466 TRUE. Missing values were imputed conservatively, with assumption of left-censored

467 distributions in each sample, using R package imputeLCMD with function impute.MinProb() with

468 $q = 0.01$ and tune.sigma = 1 to draw minimum values. BH-adjusted p-values were generated

469 with R package limma using lmFit() and eBayes().

Statistical significance

471 Quantitative analyses were performed using a two-sided Student's t-test, Mann-Whitney test,

472 One-Way ANOVA with multiple comparisons, or the Mantel-Cox test for survival using GraphPad

473 Prism. p-values of <0.05 were considered statistically significant. Statistical outliers were

474 identified by ROUT method and removed prior to analysis. All experimental conductors were

475 aware of treatment group allocations.

Author Contributions

477 All authors contributed to the study conception and design. Material preparation, data collection,

478 and analysis were performed by MP, JG, CH, and MK. The first draft of the manuscript was

479 written by MP and all authors commented on previous versions of the manuscript. All authors

480 read and approved the final manuscript.

Data Availability

482 Genomic data, including human PDAC RNA sequencing and phosphoproteomics, as well as

483 supporting materials including R code used to analyze phosphoproteomic data, are available

484 from the corresponding author upon reasonable request.

485

References

1. Oba A, Ho F, Bao QR, Al-Musawi MH, Schulick RD, Del Chiaro M. Neoadjuvant Treatment in Pancreatic Cancer. Frontiers in Oncology 2020;10 (Review) (In English). DOI: 10.3389/fonc.2020.00245.

2. Jang J-Y, Han Y, Lee H, et al. Oncological benefits of neoadjuvant chemoradiation with gemcitabine versus upfront surgery in patients with borderline resectable pancreatic cancer: a prospective, randomized, open-label, multicenter phase 2/3 trial. Annals of surgery 2018;268(2):215-222.

3. Katz MH, Shi Q, Meyers JP, et al. Alliance A021501: preoperative mFOLFIRINOX or mFOLFIRINOX plus hypofractionated radiation therapy (RT) for borderline resectable (BR) adenocarcinoma of the pancreas. American Society of Clinical Oncology; 2021.

4. Reyngold M, Karam SD, Hajj C, et al. Phase 1 Dose Escalation Study of SBRT Using 3 Fractions for Locally Advanced Pancreatic Cancer. International Journal of Radiation Oncology* Biology* Physics 2023.

5. Piper M, Van Court B, Mueller A, et al. Targeting Treg-expressed STAT3 enhances NK-mediated surveillance of metastasis and improves therapeutic response in pancreatic adenocarcinoma. Clinical Cancer Research 2022;28(5):1013-1026.

6. Barker HE, Paget JT, Khan AA, Harrington KJ. The tumour microenvironment after radiotherapy: mechanisms of resistance and recurrence. Nature Reviews Cancer 2015;15(7):409-425.

7. Piper M, Hoen M, Darragh LB, et al. Simultaneous targeting of PD-1 and IL-2Rβγ with radiation therapy inhibits pancreatic cancer growth and metastasis. Cancer Cell 2023;41(5):950-969. e6.

8. Yang Y, Lundqvist A. Immunomodulatory Effects of IL-2 and IL-15; Implications for Cancer Immunotherapy. Cancers (Basel) 2020;12(12) (In eng). DOI: 10.3390/cancers12123586.

9. Waldmann TA. The shared and contrasting roles of IL2 and IL15 in the life and death of normal and neoplastic lymphocytes: implications for cancer therapy. Cancer Immunol Res 2015;3(3):219-27. (In eng). DOI: 10.1158/2326-6066.Cir-15-0009.

10. Guo Y, Luan L, Patil NK, Sherwood ER. Immunobiology of the IL-15/IL-15Rα complex as an antitumor and antiviral agent. Cytokine Growth Factor Rev 2017;38:10-21. (In eng). DOI: 10.1016/j.cytogfr.2017.08.002.

11. Hawes RH, Xiong Q, Waxman I, Chang KJ, Evans DB, Abbruzzese JL. A multispecialty approach to the diagnosis and management of pancreatic cancer. The American journal of gastroenterology 2000;95(1):17-31.

12. Smeenk HG, Incrocci L, Kazemier G, et al. Adjuvant 5-FU-based chemoradiotherapy for patients undergoing R-1/R-2 resections for pancreatic cancer. Digestive surgery 2006;22(5):321-328.

13. Soares KC, Foley K, Olino K, et al. A preclinical murine model of hepatic metastases. JoVE (Journal of Visualized Experiments) 2014(91):e51677.

14. Jarjour NN, Wanhainen KM, Peng C, et al. Responsiveness to interleukin-15 therapy is shared between tissue-resident and circulating memory CD8(+) T cell subsets. Proc Natl Acad Sci U S A 2022;119(43):e2209021119. (In eng). DOI: 10.1073/pnas.2209021119.

15. White JT, Cross EW, Burchill MA, et al. Virtual memory T cells develop and mediate bystander protective immunity in an IL-15-dependent manner. Nat Commun 2016;7:11291. (In eng). DOI: 10.1038/ncomms11291.

16. Codarri Deak L, Nicolini V, Hashimoto M, et al. PD-1-cis IL-2R agonism yields better effectors from stem-like CD8+ T cells. Nature 2022;610(7930):161-172.

17. Tichet M, Wullschleger S, Chryplewicz A, et al. Bispecific PD1-IL2v and anti-PD-L1 break tumor immunity resistance by enhancing stem-like tumor-reactive CD8+ T cells and reprogramming macrophages. Immunity 2023;56(1):162-179. e6.

533 18.   Kratchmarov R, Magun AM, Reiner SL. TCF1 expression marks self-renewing human CD8(+) T
534   cells. Blood Adv 2018;2(14):1685-1690. (In eng). DOI: 10.1182/bloodadvances.2018016279.
535 19.   Renkema KR, Huggins MA, Borges da Silva H, Knutson TP, Henzler CM, Hamilton SE. KLRG1(+)
536   Memory CD8 T Cells Combine Properties of Short-Lived Effectors and Long-Lived Memory. J
537   Immunol 2020;205(4):1059-1069. (In eng). DOI: 10.4049/jimmunol.1901512.
538 20.   Yeo MG, Oh HJ, Cho HS, Chun JS, Marcantonio EE, Song WK. Phosphorylation of Ser 21 in Fyn
539   regulates its kinase activity, focal adhesion targeting, and is required for cell migration. J Cell
540   Physiol 2011;226(1):236-47. (In eng). DOI: 10.1002/jcp.22335.
541 21.   Gattinoni L, Ji Y, Restifo NP. Wnt/beta-catenin signaling in T-cell immunity and cancer
542   immunotherapy. Clin Cancer Res 2010;16(19):4695-701. (In eng). DOI: 10.1158/1078-0432.Ccr-
543   10-0356.
544 22.   Li X, Xiang Y, Li F, Yin C, Li B, Ke X. WNT/β-Catenin Signaling Pathway Regulating T Cell-
545   Inflammation in the Tumor Microenvironment. Front Immunol 2019;10:2293. (In eng). DOI:
546   10.3389/fimmu.2019.02293.
547 23.   Potapova TA, Daum JR, Byrd KS, Gorbsky GJ. Fine tuning the cell cycle: activation of the Cdk1
548   inhibitory phosphorylation pathway during mitotic exit. Mol Biol Cell 2009;20(6):1737-48. (In
549   eng). DOI: 10.1091/mbc.e08-07-0771.
550 24.   Wells AD. Cyclin-dependent kinases: molecular switches controlling anergy and potential
551   therapeutic targets for tolerance. Semin Immunol 2007;19(3):173-9. (In eng). DOI:
552   10.1016/j.smim.2007.02.009.
553 25.   Beltra JC, Manne S, Abdel-Hakeem MS, et al. Developmental Relationships of Four Exhausted
554   CD8(+) T Cell Subsets Reveals Underlying Transcriptional and Epigenetic Landscape Control
555   Mechanisms. Immunity 2020;52(5):825-841.e8. (In eng). DOI: 10.1016/j.immuni.2020.04.014.
556 26.   Thaventhiran JE, Fearon DT, Gattinoni L. Transcriptional regulation of effector and memory CD8+
557   T cell fates. Curr Opin Immunol 2013;25(3):321-8. (In eng). DOI: 10.1016/j.coi.2013.05.010.
558 27.   Shan Q, Li X, Chen X, et al. Tcf1 and Lef1 provide constant supervision to mature CD8(+) T cell
559   identity and function by organizing genomic architecture. Nat Commun 2021;12(1):5863. (In
560   eng). DOI: 10.1038/s41467-021-26159-1.
561 28.   Berger A, Colpitts SJ, Seabrook MSS, et al. Interleukin-15 in cancer immunotherapy: IL-15
562   receptor complex versus soluble IL-15 in a cancer cell-delivered murine leukemia model. J
563   Immunother Cancer 2019;7(1):355. (In eng). DOI: 10.1186/s40425-019-0777-8.
564 29.   Chen W, Liu N, Yuan Y, et al. ALT-803 in the treatment of non-muscle-invasive bladder cancer:
565   Preclinical and clinical evidence and translational potential. Front Immunol 2022;13:1040669. (In
566   eng). DOI: 10.3389/fimmu.2022.1040669.
567 30.   Wrangle JM, Velcheti V, Patel MR, et al. ALT-803, an IL-15 superagonist, in combination with
568   nivolumab in patients with metastatic non-small cell lung cancer: a non-randomised, open-label,
569   phase 1b trial. Lancet Oncol 2018;19(5):694-704. (In eng). DOI: 10.1016/s1470-2045(18)30148-7.
570 31.   Ring AM, Lin J-X, Feng D, et al. Mechanistic and structural insight into the functional dichotomy
571   between IL-2 and IL-15. Nature immunology 2012;13(12):1187-1195.
572 32.   Liu B, Zhu X, Kong L, et al. Bifunctional TGF-β trap/IL-15 protein complex elicits potent NK cell
573   and CD8(+) T cell immunity against solid tumors. Mol Ther 2021;29(10):2949-2962. (In eng). DOI:
574   10.1016/j.ymthe.2021.06.001.
575 33.   Xu Y, Carrascosa LC, Yeung YA, et al. An Engineered IL15 Cytokine Mutein Fused to an Anti-PD1
576   Improves Intratumoral T-cell Function and Antitumor Immunity. Cancer Immunol Res
577   2021;9(10):1141-1157. (In eng). DOI: 10.1158/2326-6066.Cir-21-0058.
578 34.   Qiu W, Su GH. Development of orthotopic pancreatic tumor mouse models. Pancreatic Cancer:
579   Springer; 2013:215-223.

580   35.   Petit V, Massonnet G, Maciorowski Z, et al. Optimization of tumor xenograft dissociation for the
581   profiling of cell surface markers and nutrient transporters. Lab Invest 2013;93(5):611-21. (In
582   eng). DOI: 10.1038/labinvest.2013.44.
583   36.   Somanchi SS, McCulley KJ, Somanchi A, Chan LL, Lee DA. A novel method for assessment of
584   natural killer cell cytotoxicity using image cytometry. PLoS One 2015;10(10):e0141074.
585   37.   Kim HJ, Kim T, Hoffman NJ, et al. PhosR enables processing and functional analysis of
586   phosphoproteomic data. Cell Rep 2021;34(8):108771. (In eng). DOI:
587   10.1016/j.celrep.2021.108771.
588   38.   Kim HJ, Kim T, Xiao D, Yang P. Protocol for the processing and downstream analysis of
589   phosphoproteomic data with PhosR. STAR Protoc 2021;2(2):100585. (In eng). DOI:
590   10.1016/j.xpro.2021.100585.
591   39.   Huber W, von Heydebreck A, Sültmann H, Poustka A, Vingron M. Variance stabilization applied to
592   microarray data calibration and to the quantification of differential expression. Bioinformatics
593   2002;18 Suppl 1:S96-104. (In eng). DOI: 10.1093/bioinformatics/18.suppl_1.s96.

594

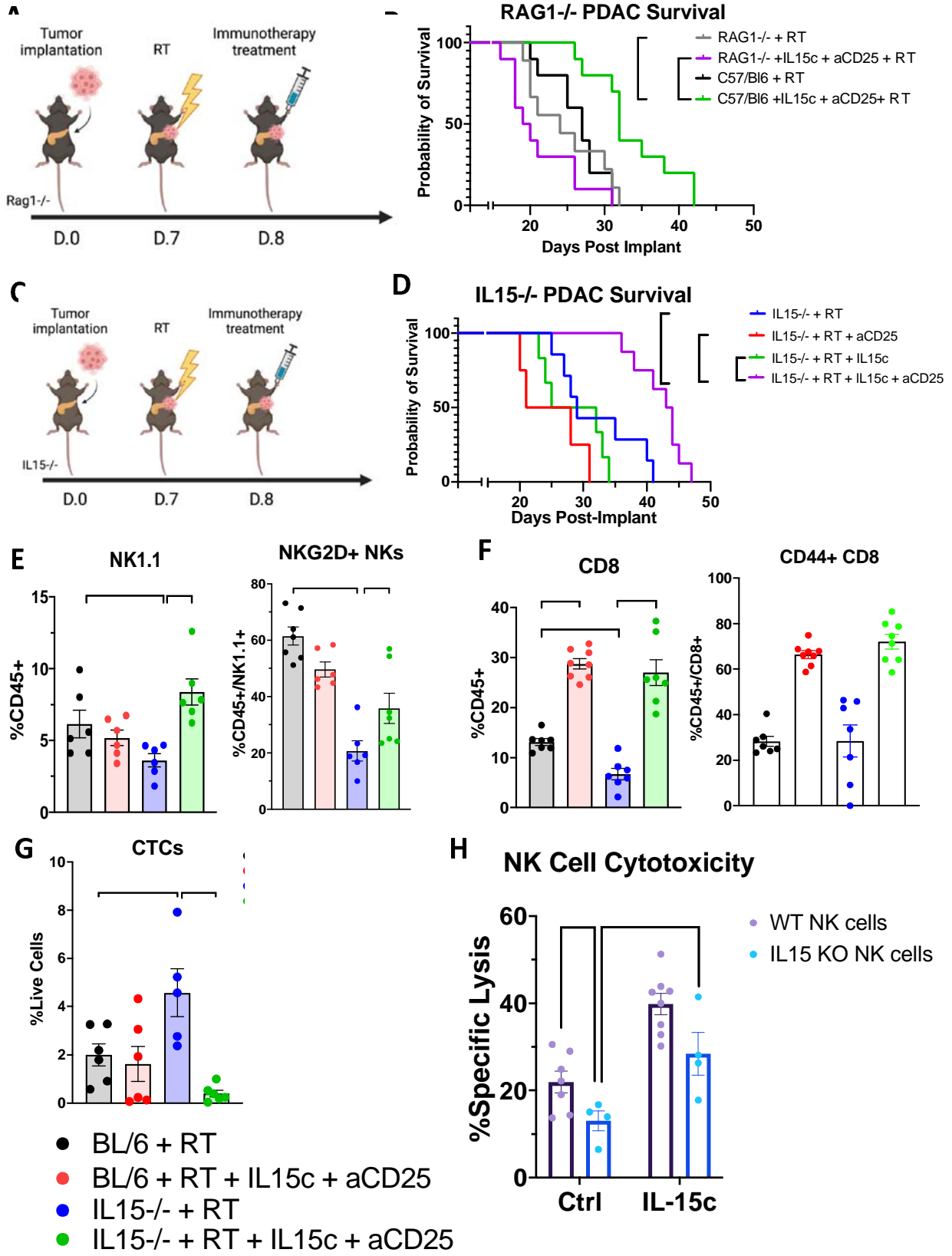# Figure 1
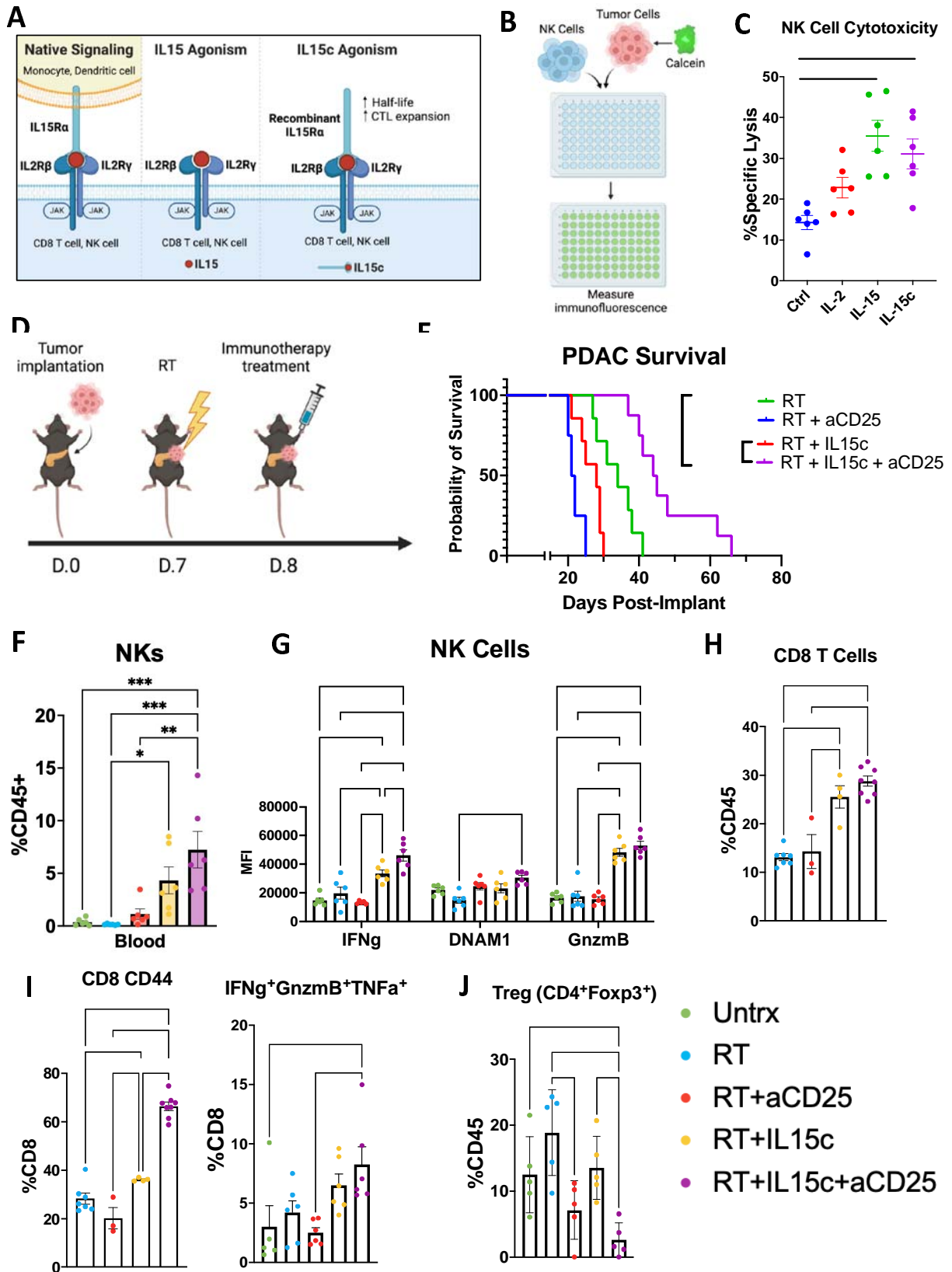
596   Figure 1:

597   a. Schematic of IL15c binding properties

598   b. Experimental design for NK cell cytotoxicity assay. n=6 per experimental group.

599   c. In vitro percent specific killing of PK5L1940 cells by C57/Bl6 derived NK cells untreated and

600   treated with IL-2, IL-15 and IL-15c as measured by calcein release.

601   d. Experimental schematic of orthotopic survival study of Fig 1E.

602   e. Kaplan-Meier survival analysis of orthotopically implanted pancreatic tumor-bearing C57/BL6

603   mice treated with RT (n=7) and IL15c (n=7), aCD25 (n=7), or IL15 + aCD25 (n=8).

604   f. Flow cytometric analysis of NK cell frequency in the blood of C57/BL6 mice treated with RT and

605   IL15c, aCD25, or IL15 + aCD25.

606   g. Flow cytometric analysis of IFNg, DNAM1, and GnzmB MFI in peripheral NK cells harvested

607   from C57BL/6 mice treated with RT and IL15c, aCD25, or IL15 + aCD25

608   h. Flow cytometric analysis of CD8 T cell frequency in the blood of C57/BL6 mice treated with RT

609   and IL15c, aCD25, or IL15 + aCD25

610   i. Flow cytometric analysis of the frequency of CD44+ (left) and IFNg+/GnzmB+/TNFa+ (right)

611   CD8 T cells in the blood of C57/BL6 mice treated with RT and IL15c, aCD25, or IL15 + aCD25.

612   j. Frequency of intratumoral Tregs in C57/BL6 mice treated with RT and IL15c, aCD25, or IL15 +

613   aCD25. n=5-6 per group for flow experiments Error bars represent SEM. $*p < 0.05$, $**p < 0.01$,

614        $***p < 0.001$, $****p < 0.0001$.

24

Figure 2
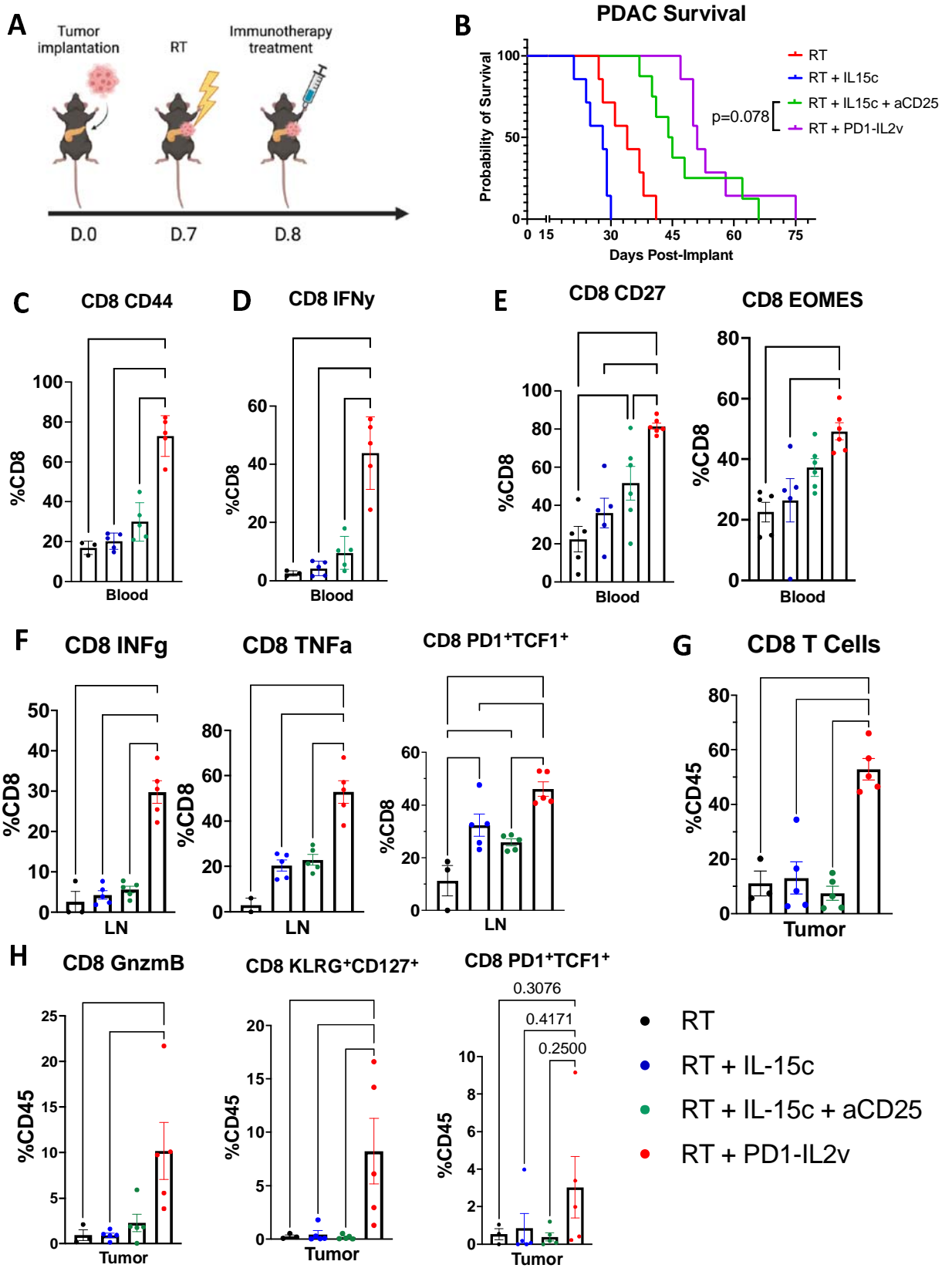
616   Figure 2

617   a.   Experimental schematic of Rag1-/- survival study in Fig 2B

618   b.   Kaplan-Meier survival analysis of orthotopically implanted pancreatic tumor-bearing C57/BL6

619   mice treated with RT (n=10) and IL15c + aCD25 (n=10) and Rag-/- mice treated with RT (n=9)

620   and IL15c + aCD25 (n=10).

621   c.   Experimental schematic of IL15-/- survival study in Fig 2D.

622   d.   Kaplan-Meier survival analysis of orthotopically implanted pancreatic tumor-bearing IL15-/-

623   mice treated with RT (n=7) and IL15c (n=6), aCD25 (n=4), or IL15 + aCD25 (n=8).

624   e.   Flow cytometric analysis of NK cell frequency (left) and NKG2D+ NK cell frequency (right) in

625   the blood of wildtype C57BL/6 and IL15-/- PDAC tumor-bearing mice treated with either RT

626   alone or RT + aCD25 + IL15c.

627   f.   Flow cytometric analysis of peripheral CD8 T cell frequency (left) and CD44+ CD8 T cell

628   frequency (right) in the blood of wildtype C57BL/6 and IL15-/- PDAC tumor-bearing mice

629   treated with either RT alone or RT + aCD25 + IL15c.

630   g.   Flow cytometric analysis of circulating tumor cell (CTC) frequency in the blood of wildtype

631   C57BL/6 and IL15-/- pancreatic tumor-bearing mice treated with either RT alone or RT + aCD25

632   + IL15c.

633   h.   In vitro percent specific killing of PDAC cancer cells by C57/BL6 and IL15-/- derived NK cells

634   untreated and treated with saline control and IL15c as measured by calcein release. n=7-8 per

635   group for flow experiments. Error bars represent SEM. $*p < 0.05$, $**p < 0.01$, $***p < 0.001$,

636        $****p < 0.0001$.

Figure 3



637

638   Figure 3

639   a. Experimental schematic of survival study in Fig 3B

640   b. Kaplan-Meier survival analysis of orthotopically implanted PDAC tumor-bearing C57/BL6 mice

641   treated with RT (n=7), RT + IL15c (n=7), RT + aCD25 + IL15c (n=8), and RT + PD1-IL2v (n=8).

642   c. Frequency of circulating CD8+/CD44+ cells as a proportion of total CD8 T cells in orthotopic

643   PDAC tumor-bearing mice treated with RT, RT + IL15c, RT + IL15c + aCD25, and RT + PD1-

644   IL2v at 21 days post-implantation

645   d. Frequency of circulating CD8+/IFNg+ cells as a proportion of total CD8 T cells in orthotopic

646   PDAC tumor-bearing mice treated with RT, RT + IL15c, RT + IL15c + aCD25, and RT + PD1-

647   IL2v at 21 days post-implantation

648   e. Frequency of circulating CD8+/CD27+ (left) and CD8+/EOMES+ (right) cells as a proportion of

649   total CD8 T cells in orthotopic PDAC tumor-bearing mice treated with RT, RT + IL15c, RT +

650   IL15c + aCD25, and RT + PD1-IL2v at 21 days post-implantation

651   f. Frequency of intramodal IFNg+ (left), TNFa+ (center), and PD1+/TCF1+ (right) CD8 T cells in

652   the draining lymph nodes of orthotopic PDAC tumor-bearing mice treated with RT, RT + IL15c,

653   RT + IL15c + aCD25, and RT + PD1-IL2v.

654   g. Frequency of intratumoral CD8 T cells as proportion of total CD45+ cells in orthotopic PDAC

655   tumor-bearing mice treated with RT, RT + IL15c, RT + IL15c + aCD25, and RT + PD1-IL2v.

656   Frequency of intratumoral GnzmB+ (left), KLGR1+/CD127+ (center), and PD1+/TCF1+ (right)

657   CD8 T cells in orthotopic PDAC tumor-bearing mice treated with RT, RT + IL15c, RT + IL15c +

658   aCD25, and RT + PD1-IL2v. n=5-6 per group for flow experiments. Error bars represent SEM.

659 $*p < 0.05$, $**p < 0.01$, $***p < 0.001$, $****p < 0.0001$.

Figure 4
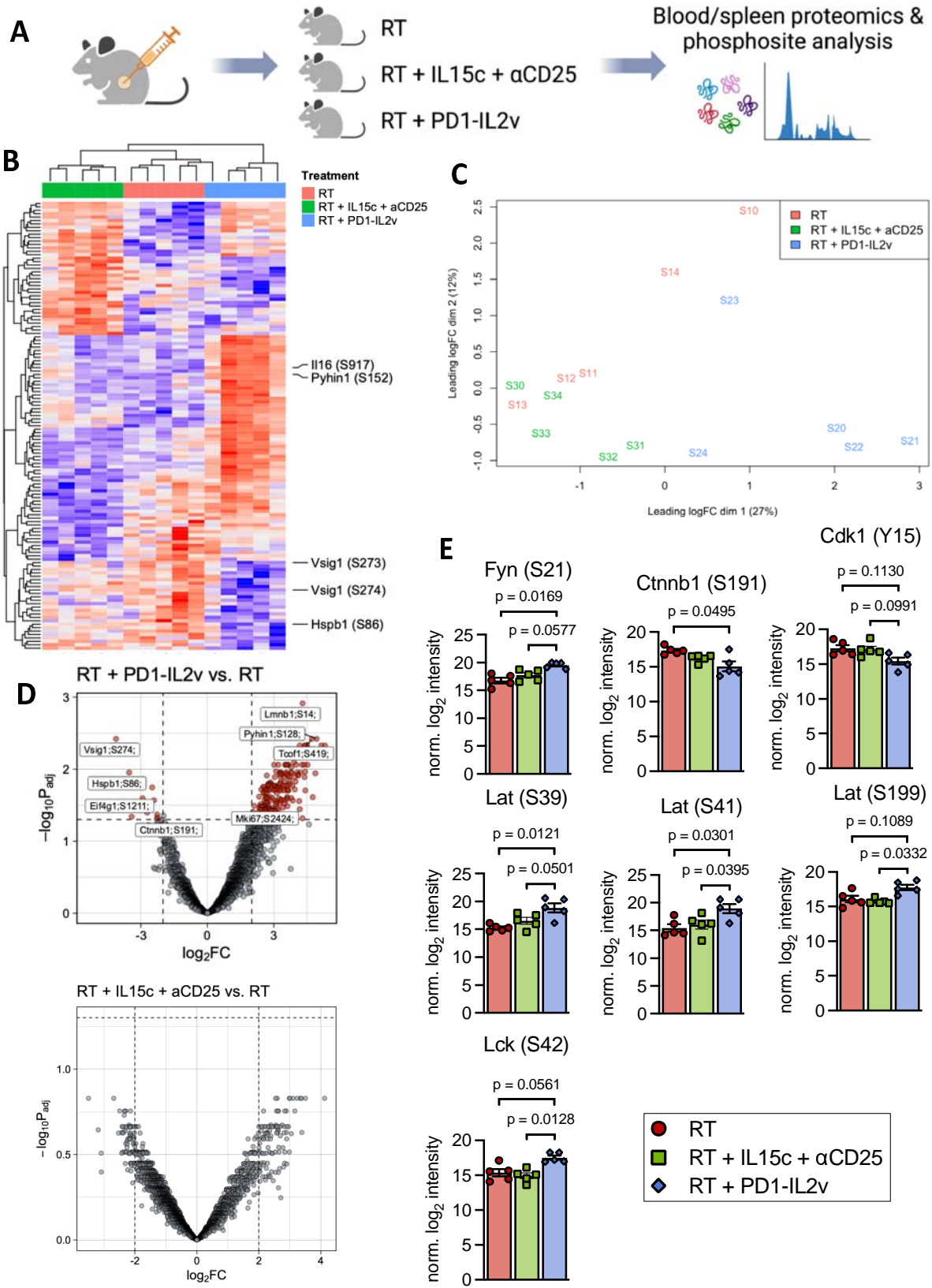
661   Figure 4

662   a.   Experimental schematic of phosphoproteomic experiment

663   b.   Hierarchal clustering of phosphites from CD8s gathered from tumor-bearing mice treated with

664   RT, RT + IL15c + aCD25, and RT + PD1-IL2v.

665   c.   PCA clustering analysis of phosphite samples from mice treated with RT, RT + IL15c + aCD25,

666   and RT + PD1-IL2v

667   d.   Volcano plots of differentially expressed phosphites in CD8 T cells of mice treated with RT vs RT

668   + PD1-IL2v (above) and RT vs RT + IL15c + aCD25 (below).

669   Expression of phosphites related to T cell signaling and activation in CD8s harvested from tumor-

670   bearing mice treated with RT, RT + IL15c + aCD25, and RT + PD1-IL2v. n=5 per group. Error

671   bars represent SEM. $*p < 0.05$, $**p < 0.01$, $***p < 0.001$, $****p < 0.0001$.
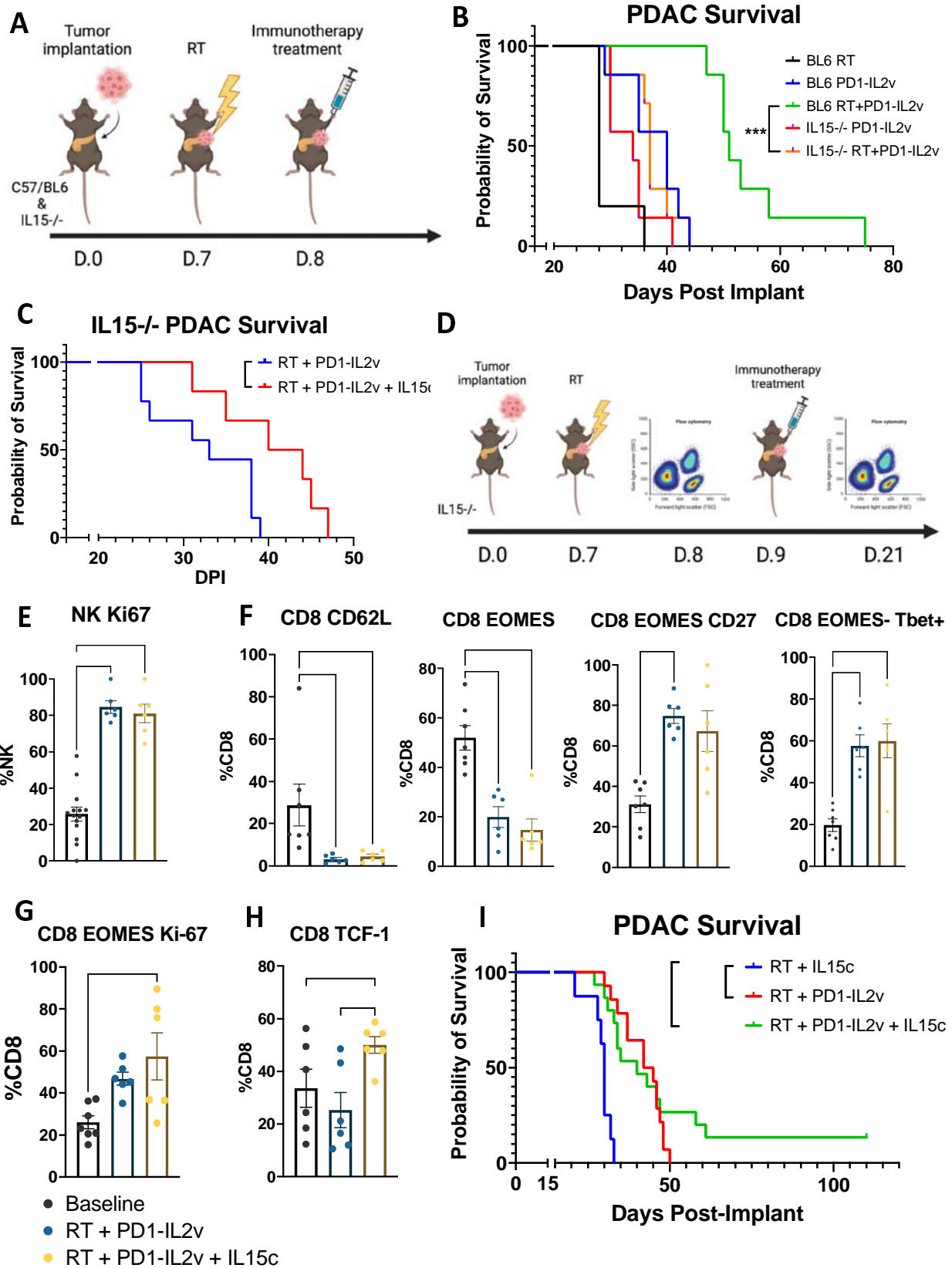
Figure 5
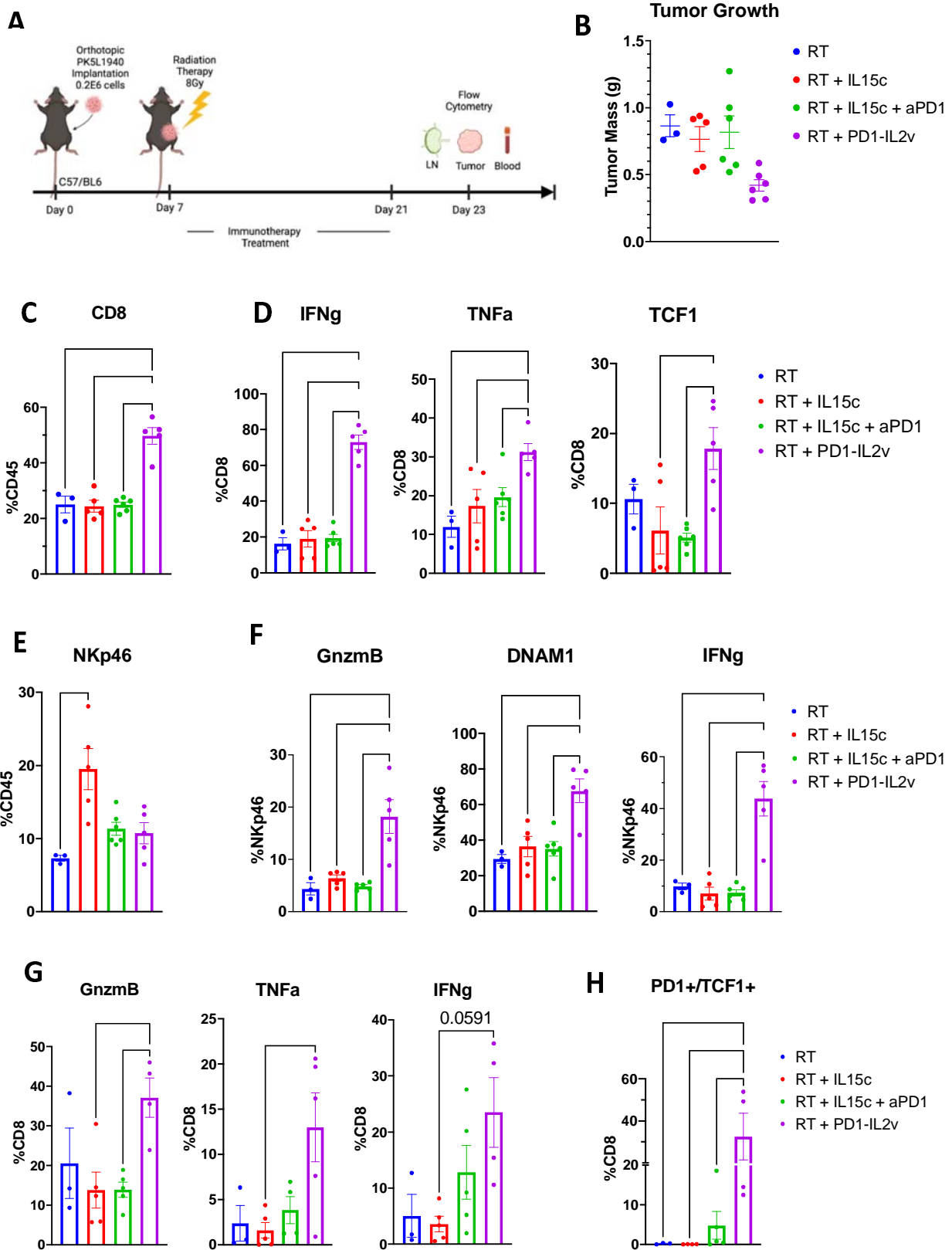
672

673

674   Figure 5:

675   a. Experimental schematic of flow cytometric analysis of intratumoral and circulating immune cells.

676   b. Mass of orthotopic pancreatic tumors treated with at day 23 post-implantation treated with

677   combinations of RT, RT+IL15c, RT+IL15c+aPD1, and RT+PD1-IL2v.

678   c. Frequency of CD8 T cells in the blood of orthotopically implanted PDAC tumor-bearing mice.

679   d. IFNg (left), TNFa (center), and TCF1 (right) expression in circulating CD8 T cells of

680   orthotopically implanted PDAC tumor-bearing mice.

681   e. Frequency of NKp46+ NK cells in the blood of orthotopically implanted PDAC tumor-bearing

682   mice.

683   f. GnzmB (left), DNAM1 (center), and IFNg (right) expression in circulating NK cells of

684   orthotopically implanted PDAC tumor-bearing mice.

685   g. Frequency of GnzmB+ (left), TNFa+ (center), and IFNg+ (right) intratumoral CD8 T cells in

686   orthotopically implanted PDAC tumor-bearing mice.

687   Frequency of intratumoral PD1+/TCF1+ progenitor exhausted CD8 T cells in orthotopically

688   implanted PDAC tumor-bearing mice. n=3-6 per group for flow experiments. Error bars

689   represent SEM. $*p < 0.05$, $**p < 0.01$, $***p < 0.001$, $****p < 0.0001$.

Figure 6

690

691

692   Figure 6:

693   a. Experimental schematic of survival study in Fig 5B

694   b. Kaplan-Meier survival analysis of orthotopically implanted PDAC tumor-bearing C57/BL6 and

695   IL15-/- mice treated with PD1-IL2v or RT + PD1-IL2v (n=5-7 per group).

696   c. Kaplan-Meier survival analysis of orthotopically implanted PDAC tumor-bearing IL15-/- mice

697   treated with RT + PD1-IL2v (n=9) and RT + PD1-IL2v + IL15c (n=6).

698   d. Experimental design of flow cytometry study in Fig 5E-H.

699   e. Frequency of Ki67+ NK cells in the blood of IL15-/- orthotopic PDAC tumor-bearing mice

700   treated with RT + PD1-IL2v (n=6) and RT + PD1-IL2v + IL15c (n=6) at baseline and following

701   the initiation of treatment.

702   f. Frequency of CD62L+, EOMES+, EOMES+/CD27+, and EOMES-/Tbet+ CD8 T cells in the

703   blood of IL15-/- orthotopic PDAC tumor-bearing mice treated with RT + PD1-IL2v (n=6) and RT

704   + PD1-IL2v + IL15c (n=6) at baseline and following the initiation of treatment.

705   g. Frequency EOMES+/Ki67+ CD8 T cells in the blood of IL15-/- orthotopic PDAC tumor-bearing

706   mice treated with RT + PD1-IL2v (n=6) and RT + PD1-IL2v + IL15c (n=6) at baseline and

707   following the initiation of treatment.

708   h. Frequency of TCF1+ CD8 T cells in the blood of IL15-/- orthotopic PDAC tumor-bearing mice

709   treated with RT + PD1-IL2v (n=6) and RT + PD1-IL2v + IL15c (n=6) at baseline and following

710   the initiation of treatment.

711   Kaplan-Meier survival analysis of orthotopically implanted PDAC tumor-bearing C57/BL6 mice

712   treated with RT + IL15c (n=8), RT + PD1-IL2v (n=14), and RT + PD1-IL2v + IL15c (n=16).

713   Error bars represent SEM. $*p < 0.05$, $**p < 0.01$, $***p < 0.001$, $****p < 0.0001$.